CARBON 50 (2012) 1727–1733

Available at www.sciencedirect.com

SciVerse ScienceDirect

journal homepage: www.elsevier.com/locate/carbon

The influence of atmosphere on electrical transport in graphene

Yinxiao Yang [a,*], Kevin Brenner [a], Raghu Murali [b]

[a] Electrical and Computer Engineering, Georgia Institute of Technology, 777 Atlantic Drive NW, Atlanta, GA 30332, USA
[b] Nanotechnology Research Center, Georgia Institute of Technology, 791 Atlantic Drive NW, Atlanta, GA 30332, USA

ARTICLE INFO

Article history:
Received 23 March 2011
Accepted 4 December 2011
Available online 11 December 2011

ABSTRACT

The effect of atmospheric adsorbates, composed of dry oxygen (O_2) and ambient air, on electrical transport in high-quality and moderate-quality graphene samples was investigated. Atmospheric doping is seen to affect different samples at different rates but in all samples hole-doping is observed within several minutes of O_2 or ambient exposure. After an initial rapid increase, the doping rate falls off dramatically. It is shown that carrier mobility (μ) can be either improved or degraded depending on the nature of the impurities affecting transport. The former case represents the first experimental demonstration of an improvement in carrier mobility with increased doping in graphene. A model is derived to understand the interplay between charge screening and impurity scattering. The study points to the possibility that oxygen and water molecules mitigate carrier scattering from negatively-charged impurities but cause increased carrier scattering from positively-charged impurities.

1. Introduction

Owing to its 2D-nature, graphene offers the ultimate surface area to volume ratio – this makes the material an ideal sensing platform. However, such sensitivity also demands the meticulous processing and handling of samples so that unintentional alteration of material properties is minimized. Not long after the first graphene devices were measured, a steady stream of doping studies and a range of sensing studies followed. These studies have usually involved the flow of a particular gas species [1–4], doping from a species in solution [5–8] or by chemical substitution [9]. Another study [10] examined the ambient effects on noise characteristics of graphene. While it is recognized that exposure of graphene to atmosphere leads to a change in electrical properties, there have been no reported studies dedicated to atmospheric effects on graphene's electrical transport. The response of graphene in atmosphere is important for many reasons: graphene device fabrication largely involves a number of steps that expose it to atmosphere, graphene performance in atmosphere is important for its use in real-time gas sensing, and many doping studies on graphene expose it to atmosphere before the doping step.

Based on previous experiments, the following points are evident. First, carrier transport in graphene is influenced by short and long-range scattering for high and low carrier density, respectively. The crossover between the two regimes is marked by the transition from linear-in-density conductance (long-range scattering) to sub-linear conductance (short-range scattering). Second, conductivity approaches 4 e^2/h only in samples with large impurity density (n_{imp}). For cleaner samples, this conductivity minimum (σ_{min}) is larger and more sensitive to fluctuations of impurity density. Moreover, the conductivity plateau at the neutrality point is determined by inhomogeneous charge puddles [11–14]. Third, doping influences graphene by introducing extra charges as well as

* *Corresponding author.*
E-mail address: yinxiao.yang@gatech.edu (Y. Yang).
0008-6223/$ - see front matter
doi:10.1016/j.carbon.2011.12.008

scattering sites, thereby increasing the charge density but also causing additional scattering which may decrease mobility.

Chen et al. [15] studied ionic screening of substrate impurities by exposing graphene to a solution of NaF. As a result, the gate voltage at which conductivity is minimum ($V_{g,min}$) shifts from +30 V to very near 0 V and mobility improves. These results fit neatly into long-range scattering theory: effects of charged impurities (from the substrate) are neutralized via ionic screening and this leads to an improvement in mobility. Also, increased potassium doping of graphene [1] is seen to degrade mobility by an order of magnitude as $V_{g,min}$ shifts from −9 V to −80 V. Generally, various dopants may improve transport by acting as compensators [16], i.e., they reduce impurity scattering in the system by neutralizing existing impurities and improve mobility. Interestingly, all previous work points to a decrease (increase) in mobility with an increase (decrease) in doping. This suggests that it is difficult to employ a dopant species as a charge screening layer while simultaneously achieving high doping densities. Our findings show that, with increasing O_2 or ambient exposure, hole-doping increases (i.e., $V_{g,min}$ shifts to more positive voltages) while hole mobility (μ_{hole}) can increase or decrease depending on sample quality. Hence, a unique result of this work is that this is the first experimental demonstration showing that dopants (atmospheric adsorbates) can compensate for impurities while at the same time improve mobility in graphene. This provides a practical and powerful counter example to the accepted notion that increased graphene doping is associated with a decreased mobility.

2. Experimental setup

Exfoliated graphene (from Kish graphite) is prepared on a 300 nm SiO_2/Si substrate. After identification of suitable graphene sheets, we use Raman spectroscopy to confirm sample thickness. Also, we note the absence of a D band, an indication of high crystalline order in the graphene lattice [17]. Metal electrodes (a stack of 10/90 nm of Ti/Au) are deposited onto graphene by e-beam lithography and a metal liftoff process. These 2-D graphene sheets are then directly used in our atmospheric doping experiments. We avoid further lithographic patterning to shape the graphene sheets in order to minimize sample contamination. A degenerately-doped silicon substrate allows for back-gating of the graphene samples, whereby the induced carrier density, n, is related to the applied back-gate voltage, V_{BG}, by the relation $n = C_{ox} \cdot V_{BG}/e$ (C_{ox} = 11.5 nF/cm^2 for the 300 nm SiO_2 dielectric used in this work).

A number of samples were studied and four cases involving three distinct samples (labeled D1-D3) are presented – these four cases cover the range of behavior observed when graphene is exposed to dry oxygen and moist air, Fig. 1. The cases also cover a range of sample quality, as indicated by carrier mobility. It is our intention to look at the behavior of not just high-quality samples since we are interested in a comprehensive evaluation of the influence of atmospheric contamination. Two different types of runs were performed with D1. Prior to both runs, the samples are pumped under vacuum (pressure $\leqslant 1 \times 10^{-5}$ mbar) for more than 10 h to drive out residual adsorbates. In the first run, termed run-A, the test chamber is opened, leaving the sample exposed to ambient air with 55% relative humidity, the conditions of our lab (at this humidity level, water vapor accounts for 1% of the ambient air by mass). In the second run, run-B, the sample is exposed to both O_2 and ambient air. Initially, the sample remains inside the test chamber while oxygen of 99.99% purity is introduced at a rate of 10 sccm. During O_2 exposure, the pump is disconnected so the chamber pressure increases with the inflow of O_2; the chamber pressure reaches 0.5 mbar after 15 min and atmospheric pressure after 30 min. Once at atmospheric pressure, the chamber remains closed so the graphene continues to be exposed to pure O_2. After nearly two hours of O_2 exposure, the flow is cut off; the test chamber is opened and the sample is exposed to ambient air for further testing. D2 and D3 are subject to run-A only.

Controlled atmospheric exposure and back-gated electrical testing is carried out under the two prescribed environmental conditions using a vacuum probe station (Lakeshore Cryogenics). In addition, a four-point probe setup (using a lock-in amplifier with an excitation current of 10 nA) is used to reduce measurement errors arising from the contacts. *I*–*V* testing, carried out at room temperature, is performed every 2 min for several hours for each doping experiment. Concerns over the possible breakdown of the gate dielectric limited the applied back-gate voltage to be swept within the range of −60 V to +60 V.

3. Results

Case 1: A moderate-quality sample (D1) is subject to run-A. Ambient doping of graphene affects conductivity in the following manner. Initially, the sample is at $V_{g,min}$ = +10 V, and σ_{min} = 8.5 e^2/h; after 141 min of exposure, $V_{g,min}$ = + 46 V and σ_{min} has decreased to 5.5 e^2/h. D1 has a width of 16 μm and length of 4 μm.

Case 2: D1, having undergone vacuum desorption to reverse the effects of run-A, is subject to run-B. After 9 min of exposure, $V_{g,min}$ = +10 V and σ_{min} = 7.9 e^2/h; after 110 min of exposure $V_{g,min}$ = +26 V and σ_{min} = 6.6 e^2/h. At this point, O_2 flow is discontinued and the sample is directly exposed to the ambient. The doping behavior remains qualitatively the same as before (i.e., hole-doping occurs) but the rate of doping increases. The rate of doping during ambient exposure could be higher since moisture is thought to promote hole-doping by O_2 [18]. In total (after 110 min of O_2 exposure followed by 106 min of ambient exposure), $V_{g,min}$ and σ_{min} shift to +39 V and 5.4 e^2/h, respectively.

Case 3: A different moderate-quality sample (D2) is subject to run-A. Increasing exposure to the ambient hole-dopes the sample, with $V_{g,min}$ increasing from +8 V to +31 V; σ_{min} decreases from 6.2 e^2/h to 4.5 e^2/h. Near the end of the exposure, a minor kink in the conductance curve begins to show. D2 has a width of 5 μm and length of 2 μm.

Case 4: A high-quality sample (D3) is subject to run-A. The sample shows the expected hole-doping with increasing ambient exposure. After over two hours of exposure, $V_{g,min}$ increases from −15 V to 16 V and σ_{min} remains nearly constant throughout. D3 has a width of 1 μm and length of 3 μm.

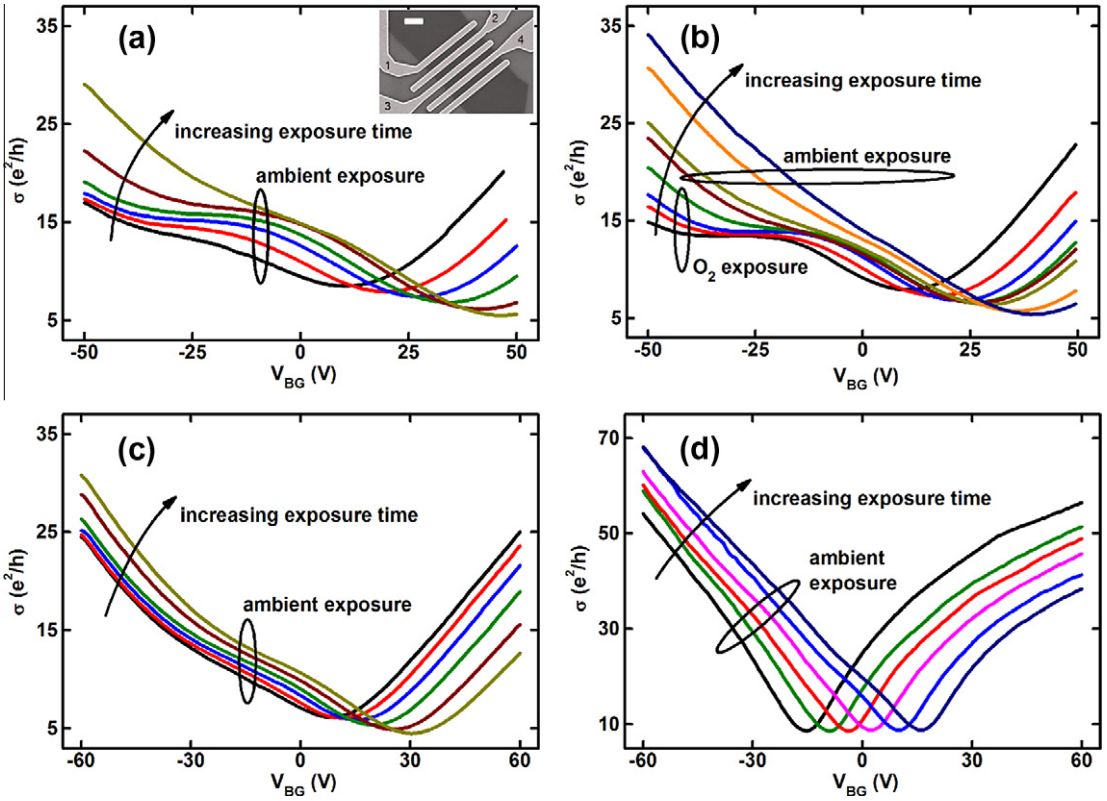

Fig. 1 – Conductivity vs. back-gate voltage, σ-V_{BG}, is plotted for three samples across four different runs. In case-1 (a), D1 is subject to run-A, or ambient exposure. σ-V_{BG} is plotted after 3, 9, 18, 36, 74, and 141 min of exposure. In case-2 (b), D1 is subject to run-B, a doping sequence using O_2 and ambient. The sample is first exposed to O_2 for 112 min, with σ-V_{BG} plotted after 9, 24, 52, and 112 min of exposure; it is then exposed to the ambient for another 104 min, with σ-V_{BG} plotted after 1, 12, 64, and 104 min of exposure. In case-3 (c), D2 is subject to run-A; σ-V_{BG} is plotted after 4, 9, 15, 39, 100, and 171 min of exposure. In case-4 (d), D3 is subject to run-A; σ-V_{BG} is plotted after 5, 10, 20, 35, 105, and 135 min of exposure (d). An SEM image of D1, with electrodes contacting the graphene sheet, is shown in the inset to (a). Four-point testing is conducted across the four electrodes denoted in the SEM image (scale bar = 1 μm).

In addition to oxygen and the ambient, we exposed our graphene samples to nitrogen. After continuous nitrogen flow (for 1 h) to the test chamber, little change in the conductance is observed. This result suggests that oxygen and water are the primary species in the atmosphere responsible for doping graphene, consistent with previous observations [19–22].

To better understand the influence of these atmospheric adsorbates on the transport, it is instructive to first consider the broader scope of scattering mechanisms in graphene. Mobility in graphene is limited by various scattering sources [23]: (i) lattice phonons that limit mobility to 2×10^5 cm^2/V-s ($\mu_{lattice}$), (ii) SiO_2 phonons that limit mobility to 4×10^4 cm^2/V-s (μ_{oxide}), and (iii) impurities (μ_{imp}). Herein, we neglect the role of edge scattering since the samples in this work have widths on the μm-scale. Using Matthiessen's rule, the total mobility can be written as:

$$\frac{1}{\mu}=\frac{1}{\mu_{lattice}}+\frac{1}{\mu_{oxide}}+\frac{1}{\mu_{imp}}. \quad (1)$$

With mobilities in the range of 1000–4000 cm^2/V-s and the predominantly linear conductance behavior at high carrier density ($n \geqslant 4\times10^{12}$ cm^{-2}), it is apparent that substrate impurities play a predominant scattering role for samples studied in this work. The assumption of impurity-limited transport allows us to express conductivity as follows [24,25]:

$$\sigma(n-\bar{n})=\begin{cases}20\cdot\frac{e^2}{h}\cdot\frac{n^*}{n_{imp}} & \text{if } n-\bar{n}\leqslant n^*\\ 20\cdot\frac{e^2}{h}\cdot\frac{n}{n_{imp}} & \text{if } n-\bar{n}>n^*\end{cases} \quad (2)$$

where n is the induced carrier density, n_{imp} is the impurity density, $\bar{n}$ is the carrier density corresponding to $V_{g,min}$, and n^* characterizes the width of the minimum conductivity plateau.

Fig. 2a plots $V_{g,min}$ vs. exposure time for the experiments of case-2 through case-4. Under atmospheric exposure, $V_{g,min}$ shifts significantly to more positive voltages, indicative of hole-doping, with the steepest shifts seen within the first 30 min of exposure. After about two hours, the capacity for the atmosphere to further hole-dope the graphene samples begins to saturate. In case-2, the doping behavior appears to show two trends; the noticeable increase in the shift of $V_{g,min}$ halfway through the entire exposure time coincides with the switch from O_2 doping to ambient doping. For all samples, it was possible to bring the *I*–*V* back to nearly its original state (before doping) after prolonged (>4 h) vacuum desorption. For example, with D1 subject to run-A, $V_{g,min}$ shifts from +10 V to +46 V. After vacuum desorption, $V_{g,min}$ falls back to

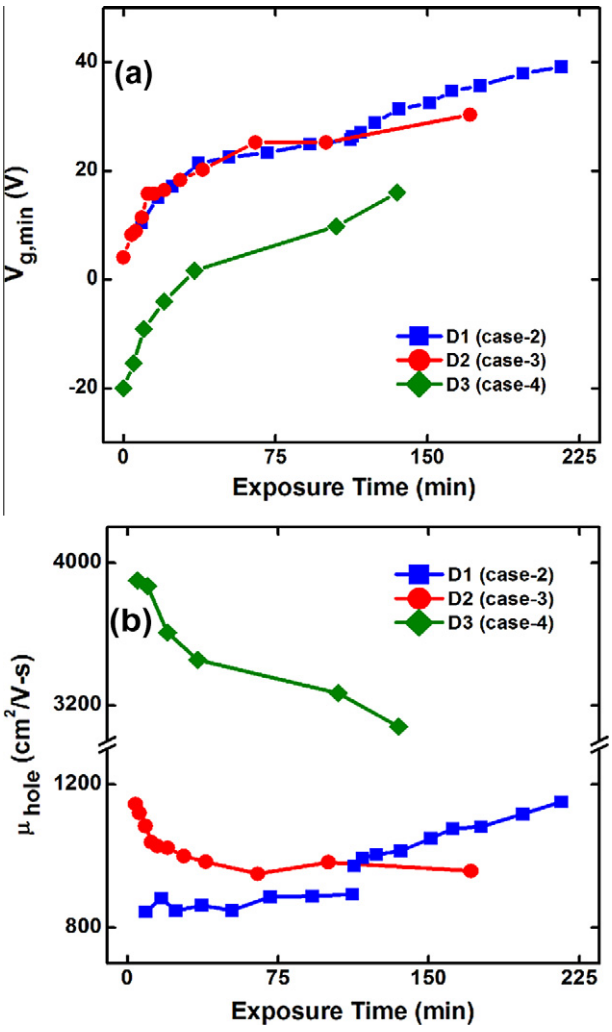

Fig. 2 – The shift in $V_{g,min}$ vs. exposure time for case-2 through case-4 is shown in (a). In (b), μ_{hole} (extracted at a hole density of 4×10^{12} cm^{-2}) vs. exposure time is shown for same set of experiments. The trend-line for case-2 is broken into two to distinguish between the response with and without O_2 flow.

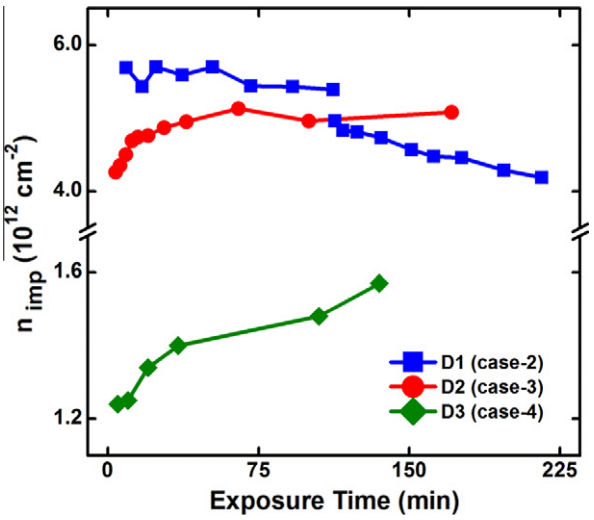

Fig. 3 – Impurity density is plotted for case-2 through case-4. The large values for n_{imp} suggest that carrier transport in our samples is largely determined by impurity scattering.

+8 V and the *I*–*V* qualitatively matches the *I*–*V* from before run-A. Given that vacuum desorption (carried out at room temperature) may restore the effects of atmospheric doping, the adsorbates interact with graphene through physisorption or a weak chemisorption process such as dipole–dipole interactions. (Note that after several cycles of atmospheric doping followed by vacuum desorption, we begin to see a small but non-reversible doping effect). This result is supported by theoretical studies which discuss a weak charge transfer between O_2 and carbon nanotubes [26,27] or between water and graphene [20,28,29]. In addition, weak chemisorption is expected to slightly modify the band structure of graphene [28], whose impact on the transport behavior observed in our samples depends on the role of weak chemisorption relative to physisorption. More aggressive desorption methods such as current annealing [30] or baking [31] can be used to study this interplay between physisorption and weak chemisorption of atmospheric adsorbates.

Next, we consider the influence of atmospheric doping on mobility, extracted via the relation $\mu = \sigma/(n\cdot e)$. In Fig. 2b, we show μ_{hole} (extracted for a hole density of 4×10^{12} cm^{-2}) vs. exposure time for case-2 through case-4. Throughout our analysis, this method of extracting μ is valid only for transport at high carrier densities. At low densities, the conductivity curves are non-linear and dominated by substrate impurities. At high densities ($n \geqslant 4\times10^{12}$ cm^{-2}), the conductivity approaches a linear-in-density form. For case-2, μ_{hole} increases by 36% – from 845 to 1152 cm^2/V-s – after 216 min of atmospheric exposure. This increase suggests that adsorbates help to compensate for substrate impurities in case-2. Meanwhile, μ_{hole} reduces by 16% after 171 min of exposure for case-3 and by 21% after 135 min of exposure for case-4.

Fig. 3a plots n_{imp} vs. exposure time for case-2 through case-4. We estimate the net impurity density using the relation in (2). In addition, we note the reciprocal relation between μ and n_{imp} by inserting (2) into the mobility expression:

$$\mu = 20\cdot\frac{e^2}{h}\cdot\frac{1}{n_{imp}\cdot e} \quad (3)$$

The calculated range of n_{imp} is from 1.2×10^{12} to 1.6×10^{12} cm^{-2} for the high-quality sample (D3) and from 4.2×10^{12} to 5.7×10^{12} cm^{-2} for the moderate-quality samples (D1 and D2).

4. Discussion

In D2 (case-3) and D3 (case-4), ambient exposure results in a decrease in μ_{hole}. On the other hand, D1 (case-2) shows an improvement in μ_{hole} with O_2 and ambient exposure; this case also features a prominent kink in the conductivity curve that disappears with increased hole-doping. Interestingly, for case-2, adsorbates play a dual role of hole dopant (expressed by a shift of $V_{g,min}$ to more positive values) and charge screening layer (expressed by an increase in carrier mobility). The former is expected since doping by oxygen or water is known to result in hole-doping [1,15,32–34]. In regards to the latter, others have shown an increase in μ accompanied by a

decrease in doping (i.e., $V_{g,min}$ shifts towards zero) [15,32] or chemical doping without affecting scattering [3]. However no one has demonstrated, to our knowledge, an occasion where an increase in μ is accompanied by an increase in doping. Herein, we find that it is possible for atmospheric adsorbates to decrease scattering from substrate impurities while at the same time increase hole-doping in graphene.

To illuminate the sample-to-sample variation and the changing behavior of each sample under atmospheric exposure, a phenomenological but physically-intuitive model is developed. We begin with the premise that – for exfoliated graphene on SiO_2 – substrate impurities lead to electron–hole puddles in the graphene sheet [11–14]. With the range of n_{imp} seen in our samples, it is apparent that transport is strongly influenced by these charge puddles. Hence, in our model the graphene sheets are divided into a collection of p- and n-regions corresponding to the type of substrate impurity dominating in that region. Several premises need to be established evenin a basic model such as this. First, what parameters should be assumed for the p- and n-regions? To simplify the model, all p-regions are assumed to be homogeneous, as are all n-regions, though the two regions are quite distinct from one another. Second, should we use percolation theory or a resistor network [35] to model the transport properties? We choose the latter since it has been shown that percolation theory is not needed to model the system of impurities affecting graphene conductance [36]; p–n junctions are modeled to be ballistic. And third, using a resistor network model, how many regions should be assumed to be p-type, how many to be n-type, and how should they be configured? We perform a few case studies – for instance, p- and n-regions or p-, n-, and p-regions connected in series – to identify which configuration gives the best fit to the experimental data.

The conductivity of each distinct p- and n-region, adapted from the expression in (2), is modeled as:

$$\sigma(V_{BG}) = \begin{cases} \sigma_{min} & \text{if } V_{BG} - V_{g,min} \leqslant V^* \\ \sigma_{min} + s \cdot \left(|V_{BG} - V_{g,min}| - V^*\right) & \text{if } V_{BG} - V_{g,min} > V^* \end{cases} \quad (4)$$

where V^* characterizes the width of the minimum conductivity plateau, an indication of sample quality. In each region, the adjustable parameters $V_{g,min}$, σ_{min} and s are found semi-empirically. Where possible, $V_{g,min}$ and σ_{min} reflect the experimental data. For instance, the position of the kink and minimum conductivity point of case-2 guides the selection of $V_{g,min}$ and σ_{min} for the p- and n-regions of the model. The parameter s is used as a fitting parameter to find the best fit between model and experiment. By comparing the expressions in (2) and (4), it is seen that s in (4) plays the role of $1/n_{imp}$ in (2). That is, s reveals information about sample quality (a higher s indicates a cleaner sample). Finally, V^* is related to the impurity density [24]; for the moderate-quality samples (D1 and D2), V^* is set to 6 V while for the high-quality sample (D3), V^* is set to 3 V.

The resistor network model is used to illustrate the electrical response of our samples to atmospheric exposure; the

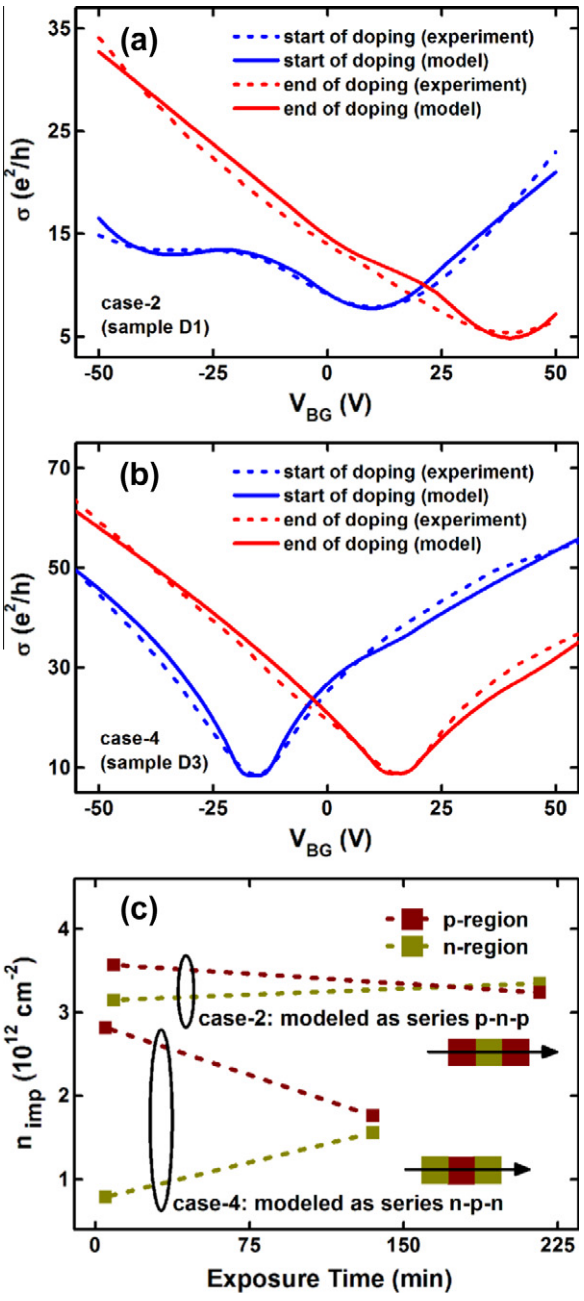

Fig. 4 – A resistor network of p- and n-regions is used to model the electrical behavior of graphene under atmospheric exposure. For D1 in case-2 (a), we find that a series connection of p-, n-, and p-regions gives a robust model that brings out the key features of the conductivity curve. For D3 in case-4 (b), we find an optimal configuration using a series connection of n-, p-, and n-regions. In each case, the model for σ vs. V_{BG} is shown at the start and end of the doping experiments; the results compare well to experimental data. In (c), we plot n_{imp} vs. exposure time for the p- and n-regions represented by the models for case-2 and case-4. It is seen that the p-regions show a decrease in n_{imp} with increasing atmospheric exposure. Finally, we illustrate the configuration of p- and n-regions used to model either case.

model fitting is performed at the beginning and end of the exposure. Fig. 4a–b compares σ vs. V_{BG} as generated by our model with the experimental data for case-2 and case-4. For D1 in case-2 (Fig. 4a), we find that a series connection of p-, n-, and p-regions leads to a robust model that brings out the key features of the conductivity curve. The model is able to portray the kink behavior observed at the start of the exposure and the disappearance of the kink at the end of the exposure. For D3 in case-4 (Fig. 4b), we find an optimal configuration using a series connection of n-, p-, and n-regions. In Fig. 4c, we plot n_{imp} vs. exposure time for the p- and n-regions in case-2 and case-4; n_{imp} changes with doping as a result of charge transfer from the adsorbates to the graphene. Herein, n_{imp} can be viewed as an effective impurity density that characterizes the combined doping from the adsorbates and the substrate impurities, as well as the interactions between adsorbates and impurities. Comparing n_{imp} before and after doping for case-2, it is seen that n_{imp} of the p-region decreases from 3.57×10^{12} to 3.24×10^{12} cm^{-2} while n_{imp} of the n-region increases from 3.15×10^{12} to 3.35×10^{12} cm^{-2}. Meanwhile for case-4, n_{imp} of the p-region decreases from 2.82×10^{12} to 1.76×10^{12} cm^{-2} and n_{imp} of the n-region increases from 0.79×10^{12} to 1.56×10^{12} cm^{-2}. These trends for the p- and n-regions are also seen for case-3 (not shown), which is modeled using a series p-n connection. We highlight the similar trends (that transport in p-regions improves while in n-regions it degrades) for case-2 and case-4 because the two showed sharply different responses to doping (μ_{hole} increases by 36% in case-2 while it decreases by 21% in case-4). This provides some insight into the sample-to-sample variation and the response to atmospheric doping observed in this work. All model parameters used to fit the experiments of case-2 through case-4 are listed in the Supplementary material.

That p-regions (n-regions) see a decrease (increase) in n_{imp} with increased atmospheric doping suggests that adsorbates help to mitigate (heighten) carrier scattering in the p-regions (n-regions). This behavior can be understood in terms of the interactions between adsorbates and substrate impurities. In particular, there is an interaction asymmetry in the following two cases: (i) repulsion between negatively-charged adsorbates (since these adsorbates donate holes to graphene) and negatively-charged substrate impurities (underneath p-regions of graphene) and (ii) attraction between negatively-charged adsorbates and positively-charged substrate impurities (underneath n-regions of graphene). In the first case (p-regions of graphene), two like charges are on opposite sides of the graphene sheet; their electric field components transverse to the basal plane cancel and μ increases. In the second case (n-regions of graphene), positive and negative charges are on opposite sides of the graphene sheet; as a result, carriers see a larger potential and μ decreases. Hence we expect that samples consisting mainly of p-regions would see overall μ improve, whereas samples consisting mainly of n-regions would see overall μ decrease.

Various arguments have been advanced to support the commonly observed electron–hole asymmetry in graphene, which is also evident in our samples. Novikov [37] suggests that due to attraction–repulsion asymmetry, the effect of screening can increase or decrease depending on whether the screening layer is positively or negatively charged. This asymmetry is a feature unique to scattering for relativistic particles. In our experiments, however, asymmetry in the I–V does not correlate to graphene thickness. This finding, in combination with the fact that carriers in bi- or few-layer graphene are massive, suggests that attraction–repulsion asymmetry is not responsible for the asymmetry in this work. Another perspective [38–40] identifies the contact metal to graphene work function difference as the source of asymmetry. Since our adhesion layer of Ti has a lower work-function than that of graphene, adjacent graphene regions undergo n-doping. Yet after testing various electrode configurations (invasive vs. non-invasive) without observing a significant difference in the conductance behavior, we infer that contact doping does not influence the atmospheric doping trends shown in this work. Lastly, we remark that this asymmetry is possibly due to the inherent variation of substrate impurities. At any rate, while we do not fully understand the origin of this asymmetry, this does not alter the trends of atmospheric doping on graphene transport observed in this work.

5. Conclusion

We study the transport properties of graphene exposed to atmospheric adsorbates (oxygen and water) and model the interaction between adsorbates and substrate impurities. Our results show that, with increased hole-doping from the atmosphere, either an improvement or degradation of carrier mobility occurs depending on the nature of the substrate impurities. That it is possible to increase mobility with increased doping is a surprising result in light of the fact that increased doping levels have been previously observed to degrade mobility. It is postulated that oxygen and water adsorbates interact with both positive and negative substrate impurities but only compensate for negatively-charged impurities. Whether an increase in mobility is seen then depends on the composition of substrate impurities: for graphene sheets consisting mainly of p-regions (corresponding to negatively-charged impurities in the substrate), the adsorbate layer tends to screen the substrate impurities and assists in the mitigation of carrier scattering. An understanding of the interplay between graphene, its supporting substrate, and atmospheric adsorbates is acutely critical to the design and fabrication of graphene devices and sensing platforms.

Acknowledgements

The authors acknowledge funding from the Nanoelectronics Research Initiative through the INDEX program and the NSF (ECCS: 1001986). In addition, the authors would like to thank James Meindl for helpful discussions and his supporting role.

Appendix A. Supplementary data

Supplementary data associated with this article can be found, in the online version, at doi:10.1016/j.carbon.2011.12.008.

REFERENCES

[1] Chen JH, Jang C, Adam S, Fuhrer MS, Williams ED, Ishigami M. Charged-impurity scattering in graphene. Nat Phys 2008;4(5):377–81.
[2] Dan Y, Lu Y, Kybert NJ, Luo Z, Johnson ATC. Intrinsic response of graphene vapor sensors. Nano Lett 2009;9(4):1472–5.
[3] Schedin F, Geim AK, Morozov SV, Hill EW, Blake P, Katsnelson MI, et al. Detection of individual gas molecules adsorbed on graphene. Nat Mater 2007;6(9):652–5.
[4] Wang X, Li X, Zhang L, Yoon Y, Weber PK, Wang H, et al. N-doping of graphene through electrothermal reactions with ammonia. Science 2009;324(5928):768–71.
[5] Cheng Z, Li Q, Li Z, Zhou Q, Fang Y. Suspended graphene sensors with improved signal and reduced noise. Nano Lett 2010;10(5):1864–8.
[6] Farmer DB, Golizadeh-Mojarad R, Perebeinos V, Lin Y-M, Tulevski GS, Tsang JC, et al. Chemical doping and electron–hole conduction asymmetry in graphene devices. Nano Lett 2008;9(1):388–92.
[7] Mohanty N, Berry V. Graphene-based single-bacterium resolution biodevice and DNA transistor: interfacing graphene derivatives with nanoscale and microscale biocomponents. Nano Lett 2008;8(12):4469–76.
[8] Ohno Y, Maehashi K, Yamashiro Y, Matsumoto K. Electrolyte-gated graphene field-effect transistors for detecting pH and protein adsorption. Nano Lett 2009;9(9):3318–22.
[9] Lherbier A, Blase X, Niquet Y-M, Triozon F, Roche S. Charge transport in chemically doped 2D graphene. Phys Rev Lett 2008;101(3):036808-1–4.
[10] Rumyantsev S et al. Electrical and noise characteristics of graphene field-effect transistors: ambient effects, noise sources and physical mechanisms. J Phys Condens Matter 2010;22(39):395302-1–7.
[11] Galitski VM, Adam S, Das Sarma S. Statistics of random voltage fluctuations and the low-density residual conductivity of graphene. Phys Rev B 2007;76(24):245405-1–7.
[12] Martin J, Akerman N, Ulbricht G, Lohmann T, Smet JH, von Klitzing K, et al. Observation of electron-hole puddles in graphene using a scanning single-electron transistor. Nat Phys 2008;4(2):144–8.
[13] Rossi E, Das Sarma S. Ground state of graphene in the presence of random charged impurities. Phys Rev Lett 2008;101(16):166803-1–4.
[14] Zhang Y, Brar VW, Girit C, Zettl A, Crommie MF. Origin of spatial charge inhomogeneity in graphene. Nat Phys 2009;5(10):722–6.
[15] Chen F, Xia J, Tao N. Ionic screening of charged-impurity scattering in graphene. Nano Lett 2009;9(4):1621–5.
[16] Hwang EH, Adam S, Das Sarma S. Transport in chemically doped graphene in the presence of adsorbed molecules. Phys Rev B 2007;76(19):195421-1–6.
[17] Ferrari AC. Raman spectroscopy of graphene and graphite: disorder, electron–phonon coupling, doping and nonadiabatic effects. Solid State Commun 2007;143(1–2):47–57.
[18] Ryu S, Liu L, Berciaud S, Yu Y-J, Liu H, Kim P, et al. Atmospheric oxygen binding and hole doping in deformed graphene on a SiO_2 substrate. Nano Lett 2010;10(12):4944–51.
[19] Collins PG, Bradley K, Ishigami M, Zettl A. Extreme oxygen sensitivity of electronic properties of carbon nanotubes. Science 2000;287(5459):1801–4.
[20] Leenaerts O, Partoens B, Peeters FM. Water on graphene: hydrophobicity and dipole moment using density functional theory. Phys Rev B 2009;79(23):235440-1–5.
[21] Levesque PL, Sabri SS, Aguirre CM, Guillemette J, Siaj M, Desjardins P, et al. Probing charge transfer at surfaces using graphene transistors. Nano Lett 2010;11(1):132–7.
[22] Liu L, Ryu S, Tomasik MR, Stolyarova E, Jung N, Hybertsen MS, et al. Graphene oxidation: thickness-dependent etching and strong chemical doping. Nano Lett 2008;8(7):1965–70.
[23] Chen JH, Jang C, Xiao SD, Ishigami M, Fuhrer MS. Intrinsic and extrinsic performance limits of graphene devices on SiO_2. Nat Nanotechnol 2008;3(4):206–9.
[24] Adam S, Hwang EH, Galitski VM, Das Sarma S. A self-consistent theory for graphene transport. Proc Nat Acad of Sci 2007;104(47):18392–7.
[25] Tan YW, Zhang Y, Bolotin K, Zhao Y, Adam S, Hwang EH, et al. Measurement of scattering rate and minimum conductivity in graphene. Phys Rev Lett 2007;99(24):246803-1–4.
[26] Jhi S-H, Louie SG, Cohen ML. Electronic properties of oxidized carbon nanotubes. Phys Rev Lett 2000;85(8):1710–3.
[27] Ulbricht H, Moos G, Hertel T. Physisorption of molecular oxygen on single-wall carbon nanotube bundles and graphite. Phys Rev B 2002;66(7):075404-1–7.
[28] Ribeiro RM, Peres NMR, Coutinho J, Briddon PR. Inducing energy gaps in monolayer and bilayer graphene: local density approximation calculations. Phys Rev B 2008;78(7):075442-1–7.
[29] Wehling TO, Lichtenstein AI, Katsnelson MI. First-principles studies of water adsorption on graphene: the role of the substrate. Appl Phys Lett 2008;93(20):202110-1–3.
[30] Bolotin KI, Sikes KJ, Jiang Z, Klima M, Fudenberg G, Hone J, et al. Ultrahigh electron mobility in suspended graphene. Solid State Commun 2008;146(9–10):351–5.
[31] Ishigami M, Chen JH, Cullen WG, Fuhrer MS, Williams ED. Atomic structure of graphene on SiO_2. Nano Lett 2007;7(6):1643–8.
[32] Chen F, Xia J, Ferry DK, Tao N. Dielectric screening enhanced performance in graphene FET. Nano Lett 2009;9(7):2571–4.
[33] Lafkioti M, Krauss B, Lohmann T, Zschieschang U, Klauk H, Klitzing KV, et al. Graphene on a hydrophobic substrate: doping reduction and hysteresis suppression under ambient conditions. Nano Lett 2010;10(4):1149–53.
[34] Ponomarenko LA, Yang R, Mohiuddin TM, Katsnelson MI, Novoselov KS, Morozov SV, et al. Effect of a high-kappa environment on charge carrier mobility in graphene. Phys Rev Lett 2009;102(20):206603-1–4.
[35] Cheianov VV, Fal'ko VI, Altshuler BL, Aleiner IL. Random resistor network model of minimal conductivity in graphene. Phys Rev Lett 2007;99(17):176801-1–4.
[36] Zhang LM, Fogler MM. Nonlinear screening and ballistic transport in a graphene p–n junction. Phys Rev Lett 2008;100(11):116804-1–4.
[37] Novikov DS. Numbers of donors and acceptors from transport measurements in graphene. Appl Phys Lett 2007;91(10):102102-1–3.
[38] Blake P, Yang R, Morozov SV, Schedin F, Ponomarenko LA, Zhukov AA, et al. Influence of metal contacts and charge inhomogeneity on transport properties of graphene near the neutrality point. Solid State Commun 2009;149(27–28):1068–71.
[39] Lee EJH, Balasubramanian K, Weitz RT, Burghard M, Kern K. Contact and edge effects in graphene devices. Nat Nano 2008;3(8):486–90.
[40] Mueller T, Xia F, Freitag M, Tsang J, Avouris P. Role of contacts in graphene transistors: a scanning photocurrent study. Phys Rev B 2009;79(24):245430-1–6.